A POLYPROPYLENE CARBONATE-BASED ADAPTIVE BUFFER LAYER FOR STABLE INTERFACES OF SOLID POLYMER LITHIUM METAL BATTERIES

A Dissertation
Presented to
The Academic Faculty

by

Haochen Yang

In Partial Fulfillment
of the Requirements for the Degree
Master of Science in the
School of Chemical and Biomolecular Engineering

Georgia Institute of Technology
May 2019

Approved by:

Dr. Nian Liu, Advisor
School of Chemical and Biomolecular Engineering
Georgia Institute of Technology

Dr. Elsa Reichmanis
School of Chemical and Biomolecular Engineering
Georgia Institute of Technology

Dr. Paul Kohl
School of Chemical and Biomolecular Engineering
Georgia Institute of Technology

Date Approved: April 10, 2019

The thesis is dedicated to my dear parents.

ACKNOWLEDGEMENTS

The two-year master experience at Georgia Institute of Technology is a truly valuable, memorable, and pleasant journey for me. This experience improved my insight, capability, confidence, and courage of discovering, thinking and resolving challenges not only in scientific research and development, but also in my entire life.

Herein, I would like to firstly give thanks to my thesis advisor, Prof. Nian Liu. During these two years, I received an enormous amount of encouragement, guidance, and kind advice from him. I would not have been able to finish my project without his guidance. In addition, I would like to also express my sincere thanks to Prof. Paul Kohl and Prof. Elsa Reichmanis for agreeing to be in my thesis committee. I have learned a lot in my studies of solid polymer electrolytes for lithium batteries from them.

I truly appreciate our group members and lab-mates, especially Dr. Yizhang, Dr. Tzuho Wu, Dr. Yubin He, Yamin Zhang, Yutong Wu, Youn Ji Min, Po-Wei Huang, Peng Chen, Jiabao Li, Tianqi Hao and Yanghang Huang. Also, I would like to thank the undergraduate researcher, Zachary Althouse, for working with me for one semester. Besides, I would like to make special thanks to Michael J Tennenbaum and Prof. Alberto Fernandez-Nieves for tremendous help on my research project.

I also would like to gratefully acknowledge KOLON INDUSTRIES that provide me with a good opportunity to participate in a project about polymer electrolytes for lithium batteries.

TABLE OF CONTENTS

LIST OF FIGURES

LIST OF SYMBOLS AND ABBREVIATIONS

SPE	solid polymer electrolyte
ABL	adaptive buffer layer
Li	lithium
Li^+	lithium ion
MW	molecular weight
PPC	polypropylene carbonate
PEO	poly(ethylene oxide)
LIB	lithium ion battery
SSE	solid-state electrolyte
EIS	electrochemical impedance spectroscopy
LFP	lithium iron phosphate
LTO	lithium titanate spinel
LVO	lithium vanadates
σ	ionic conductivity
R	resistance
S	electrode area
L	electrode thickness
R_t	total resistance of full battery
σ_t	total ionic conductivity of full battery
R_b	bulk resistance
R_{int}	interface resistance
LiTFSI	bis(trifluoromethane)sulfonimide lithium salt

AN	acetonitrile
SEM	scanning electron microscopy
C_6	graphite
T_g	glass transition temperature
GPE	gel polymer electrolyte
G’(ω)	storage modulus
G’’(ω)	loss modulus
σ (t)	stress response

SUMMARY

Solid polymer electrolytes (SPEs) have the potential to enhance the safety and energy density of lithium batteries. However, the poor interfacial contact between the lithium metal anode and SPE leads to high interfacial resistance and low specific capacity of a battery. In this work, we present a novel strategy to improve this solid-solid interface problem and maintain good interfacial contact during battery cycling by introducing an adaptive buffer layer (ABL) between the Li metal anode and SPE. The ABL consists of low molecular weight polypropylene carbonate (PPC), poly(ethylene oxide) (PEO) and lithium salt. Viscoelastic properties obtained by rheology experiments indicate that ABL has better liquid-like properties than PEO SPE. The ABL also has higher ionic conductivity than PEO SPE. In the presence of ABL, the interface resistance of the Li/ABL/SPE/$LiFePO_4$ battery only increased 20% after 150 cycles, whereas that of the battery without ABL increased 117%. In addition, since ABL makes a good solid-solid interface contact between Li metal anode and SPE, the battery with ABL delivered an initial discharge specific capacity of >110 mAh/g, which is nearly twice that of the battery without ABL (60 mAh/g). Moreover, ABL is able to keep this good interfacial contact during battery cycling, which makes the Coulombic efficiency of the battery more stable.

CHAPTER 1. INTRODUCTION

1.1 Lithium Batteries

Chemical batteries have played important roles in energy storage and conversion [1, 2]. Nowadays, among all of the available battery technologies, lithium batteries are regarded as the most promising ones because of their relatively higher energy density and design flexibility [1]. In the market, rechargeable lithium ion batteries (LIBs) are one of the most mature and promising candidates among all kinds of lithium-based batteries. LIBs are key components of the portable, entertainment, computing, transportation and telecommunication equipment in modern society.

The electrode material is one of the most interesting topics in battery technology. LIBs store electrical energy in electrodes made of lithium-intercalation or insertion compounds. On the anode-side, graphite (C_6) with a theoretical capacity of 372 Ah/kg is a commercial choice. Silicon, lithium titanate spinel $Li_4Ti_5O_{12}$ (LTO) and lithium vanadates Li_3VO_4 (LVO) are also popular anodes of LIBs. On the cathode-side, lithium cobalt oxide $LiCoO_2$ with a theoretical capacity of 274 Ah/kg is a commercial choice. Besides, several alternatives to $LiCoO_2$, such as lithium manganese oxide $LiMn_2O_4$, lithium nickel oxide $LiNiO_2$ and lithium iron phosphate $LiFePO_4$, have been developed. In my master thesis project, LFP was selected as the cathode material. Olivine-structured LFP was first proposed in the late 1990s, by Padhi et al [3], and the structure of LFP is shown in Figure 1.1 [1]. This is the first cathode material using low cost, plentiful, and environmentally friendly elements such as Fe or Mn that could have a significant impact on electrochemical energy storage [1].

If we use graphite as anode material, the charge process can be described with following reactions:

Anode: $$xLi^+ + xe^- + C_6 \xrightarrow{\text{charge}} Li_xC_6 \quad (1)$$

Cathode: $$LiFePO_4 \xrightarrow{\text{charge}} Li_{1-x}FeO_4 + xLi^+ + xe^- \quad (2)$$

Cell reaction: $$C_6 + LiFePO_4 \xrightarrow{\text{charge}} LiC_6 + FePO_4 \quad (3)$$

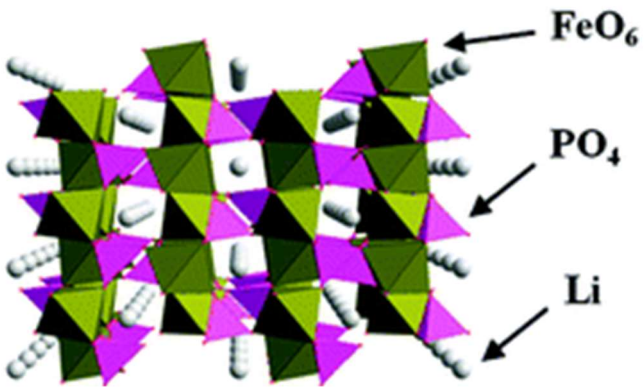

Figure 1.1. The structure of $LiFePO_4$. Reproduced with permission [2]. Copyright 2011, American Chemical Society.

Although LIBs have had a profound impact on our daily life, the inherent drawbacks of Li-ion chemistry, such as relatively low energy density, limit their further development. For these reasons, battery chemistries beyond Li-ion really need to be improved [1]. Lithium metal is an ideal choice for the anode in a lithium-based battery due to its highest theoretical capacity (3,860 mAh/g), which is more than ten times that of graphite (372 mAh/g), and lowest electrochemical potential (-3.04 V versus the standard hydrogen electrode) of all possible candidates [4,5]. Moreover, state-of-the-art Li-ion batteries can reach a specific

energy of ~250 Wh/kg, which is an order of magnitude lower than petrol (gasoline). When lithium metal is used as the anode of lithium batteries, a Li-LMO battery (M represents a transition metal, such as Co, Ni and Mn) is able to deliver a specific energy of ~440 Wh/kg. Moreover, in the Li-S and Li-air systems, they can further boost the specific energy to ~650 Wh/kg and ~950 Wh/kg, respectively [4]. The comparison of specific energy and energy density between different systems of batteries mentioned above is shown in Figure 1.2 [4].

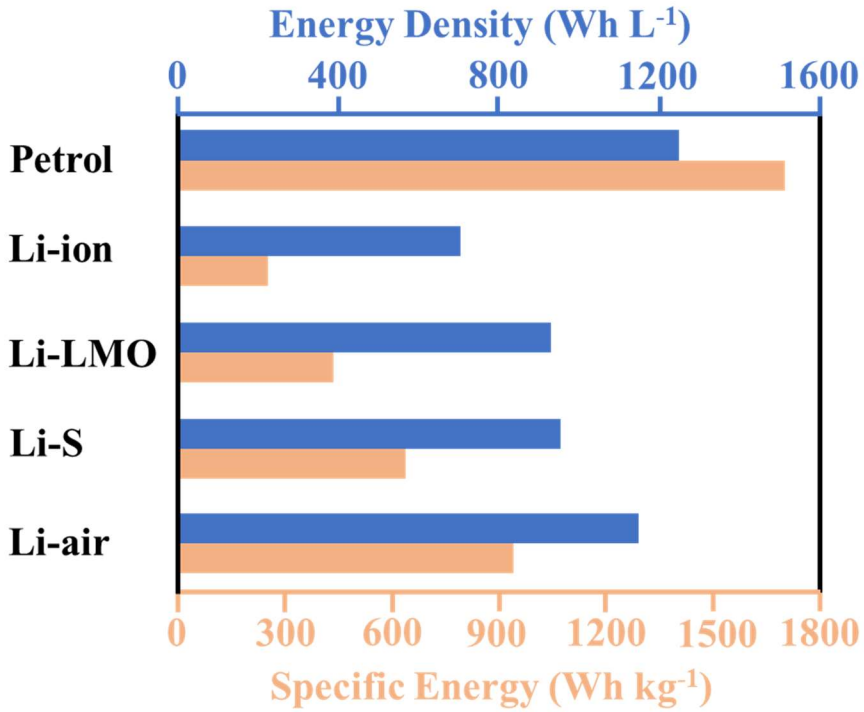

Figure 1.2. Bar chart showing the practical specific energy (pink) and energy densities (blue) of petrol (gasoline) and typical Li batteries including the state-of-the-art Li-ion battery, the Li metal/LMO cell, Li–S and Li–air cells. Reproduced with permission [4]. Copyright 2017, Nature Publishing Group.

Along with electrodes, the electrolyte is another indispensable part of a battery. Normally, conventional lithium batteries use organic liquid electrolytes, which have relatively high ionic conductivity; however, they also suffer from serious safety problems

due to their low flash point, toxicity and complex side reactions with electrodes, which inhibits their further development. Thus, studies on safer and more reliable electrolytes for lithium batteries are urgent and obligatory.

1.2 Solid-state Electrolytes (SSEs)

To solve the safety problem of the traditional organic liquid electrolyte, there is a growing interest in solid-state electrolytes for lithium batteries due to their low- or non-flammability. SSEs generally have two categories: inorganic ceramic electrolytes and solid polymer electrolytes (SPEs) [6,7]. The list of inorganic ceramic electrolytes mainly includes oxide-based ceramic electrolyte such as NASICON-Like ceramic electrolytes [8,9], garnet structure electrolytes [10], and sulfide-based ceramic electrolytes [11,12]. The organic SPEs also have various categories such as poly(ethylene oxide) (PEO)-based SPE [13], polypropylene carbonate (PPC)-based SPE [14], polysiloxane-based SPE [15-17] and single lithium-ion conducting SPE [18-20]. Compared to inorganic solid electrolytes, SPEs, in general, have better flexibility, wider electrochemical stability windows and lower cost. In my master thesis project, I focused on the research about SPEs.

The studies of SPEs started with PEO by incorporating this polymer with lithium salts to form cations and anions in an SPE system. PEO is a polyether compound with a chemical structure of H-(O-CH_2-CH_2)$_n$-OH (Figure 1.3) [21]. PEO is able to complex with lithium salt to form polymer electrolytes. The EO units have a high donor number for Li^+ and high chain flexibility for promoting rapid ion transport. The mechanism of Li^+ transport in a PEO matrix is shown in Figure 1.4 [21]. The lithium ions are coordinated by the ether oxygen atoms on a segmental PEO chain in a similar way to their complexation by organic

carbonates. Li^+ transport occurs by intrachain or interchain hopping in the PEO-based electrolyte when the lithium-oxygen bonds (Li-O) break and reform. Accompanied by the gradual replacement of the ligands for the solvation of Li^+, the continuous segmental rearrangement results in a long-range displacement of lithium ions.

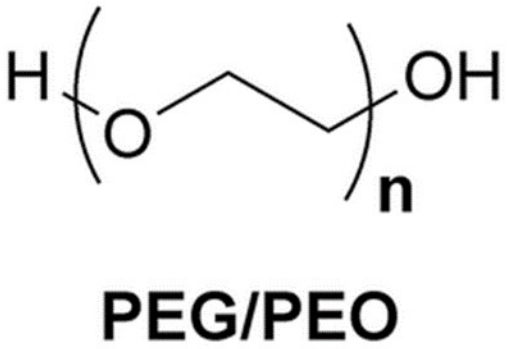

Figure 1.3. Structure of PEO. Reproduced with permission [21]. Copyright 2015, Royal Society of Chemistry.

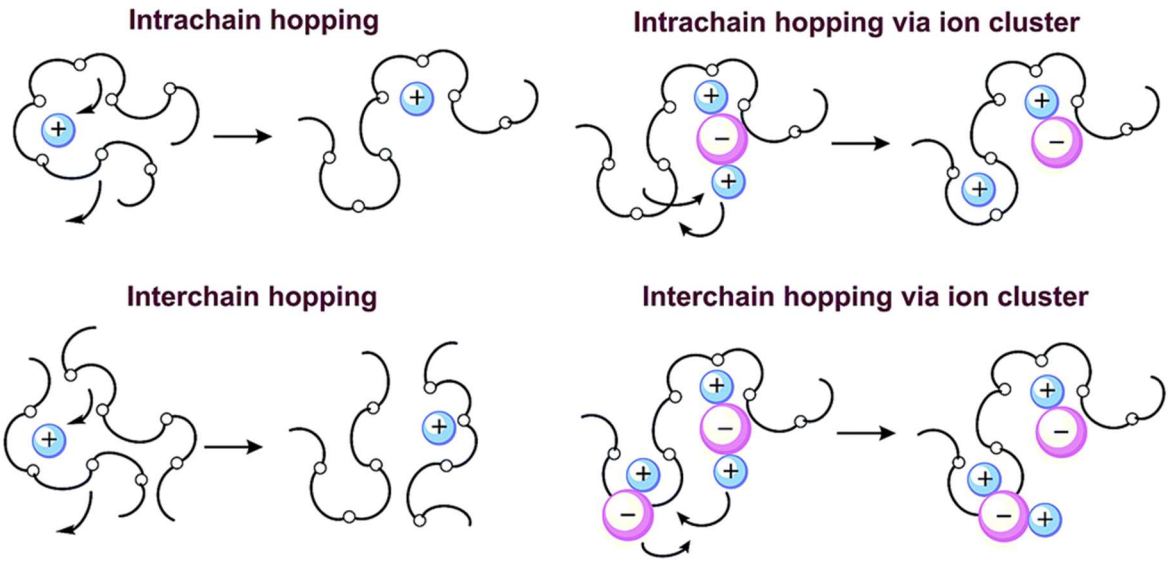

Figure 1.4. Mechanism of ion transport in PEO. Reproduced with permission [21]. Copyright 2015, Royal Society of Chemistry.

PEO is a semi-crystalline polymer, and temperature has a great impact on the activity of segmental motion in this polymer. When the temperature is higher than the glass transition temperature (T_g), the amorphous phase in PEO with activated chain segments is able to aid the transportation of Li^+. In contrast, at low temperatures (lower than T_g), the segmental motion of the polymer chains is slow, which leads to high ion resistance. The schematic morphologies of semi-crystalline PEO is shown in Figure 1.5 [21]. To obtain a satisfactory Li^+ conductivity of PEO-based electrolyte for lithium batteries, the batteries need to be run at high temperature, around the melting point (T_m), and the crystalline of polymer is melted.

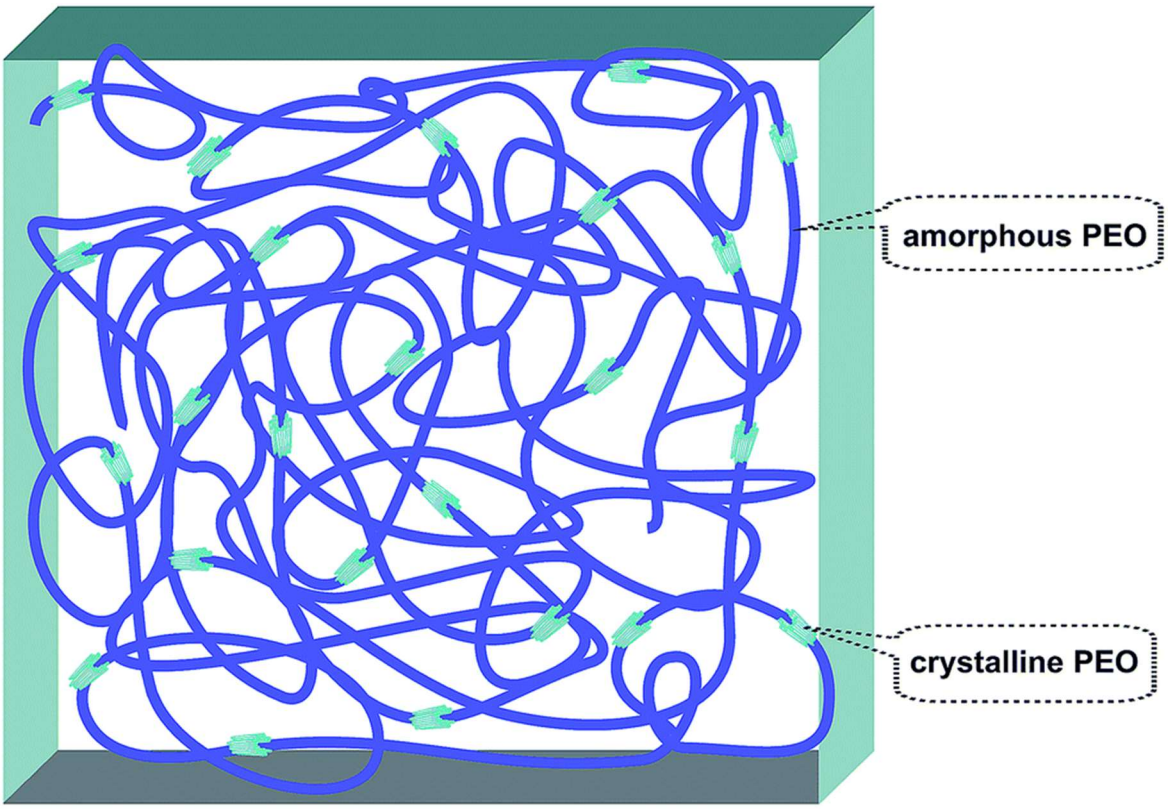

Figure 1.5. Schematic of morphologies of semi-crystalline PEO. Reproduced with permission [21]. Copyright 2015, Royal Society of Chemistry.

The low ionic conductivity of PEO-based electrolytes at ambient temperature (10^{-7} – 10^{-6} S/cm) limits their application in batteries for use in everyday life. To increase the ionic conductivity of PEO SPE, the addition of fillers such as Al_2O_3 [22], SiO_2 [23], ZnO [24], $Li_{6.75}La_3Zr_{1.75}Ta_{0.25}O_{12}$ (LLZTO) [25] and $Li_{1.3}Al_{0.3}Ti_{1.7}(PO_4)_3$ (LATP) [26] is really helpful. The large surface area of the nano-size fillers is able to prevent the recrystallization of PEO chains during the cooling process from high temperature ($>T_g$) [27]. Besides, as solid-state electrolyte, the poor solid-solid interface contact between electrode material and SPE is also a critical problem that leads to poor power density and rapid performance degradation.

1.3 Objectives

To solve the problem of poor interfacial contact between electrodes and SPE, gel polymer electrolyte (GPE), which combines the organic liquid electrolyte and polymer matrix, was introduced [28]. Because it contains the liquid electrolyte, GPE is able to have good interfacial contact with electrodes. However, the incorporation of liquid electrolyte decreases the safety of batteries.

In this work, to develop a safer strategy to improve the interfacial contact between Li metal and SPE, we designed an ABL based on polymer inspired by the concept of "self-healing". Self-healing is the ability to repair damage spontaneously and has widely used in battery technology, such as cathode materials of $LiMn_2O_4$ and $LiTi_2(PO_4)_3$ [29] and anode material of silicon [30]. As shown in Figure 1.6, for the battery without ABL, the interfacial contact between lithium metal and SPE will become poor as the surface of the lithium metal deforms during cycling. In contrast, ABL is able to maintain good

surface contact by filling the bumps and voids on lithium metal formed during batteries cycling [31]. This characteristic of ABL is attributed to low MW PPC (M.W. ~2,000 Da). PPC is a copolymer of propylene oxide and carbon dioxide and the structure of PPC is shown in Figure 1.7. As a new amorphous aliphatic polycarbonate, the local relaxation and segmental motion of PPC is favorable for the conduction of lithium ions [14]. Besides, the PPC has a lower glass transition temperature than PEO [32], which makes the PPC-based SPE a promising candidate for the ABL for the battery. Due to the low T_g, PPC-based ABL shows some semi-liquid fluidity at battery working temperature (i.e. 50 °C). During battery cycling, the PPC SPE is able to deform with the shape change of Li, so it can play a role of ABL between the Li metal anode and SPE to maintain good interfacial contact. However, the interface between pure PPC-based SPE and lithium metal anode is unstable because of the high concentration of dissociable hydroxide protons at the end of the low MW PPC chains. Moreover, the fluidity of pure PPC SPE is so high that it cannot generate a membrane and can be easily squeezed out while assembling batteries, which prevents the PPC SPE from having an impact on the battery. To address this problem, we mixed PPC and lithium salt with high MW to create my ABL [33].

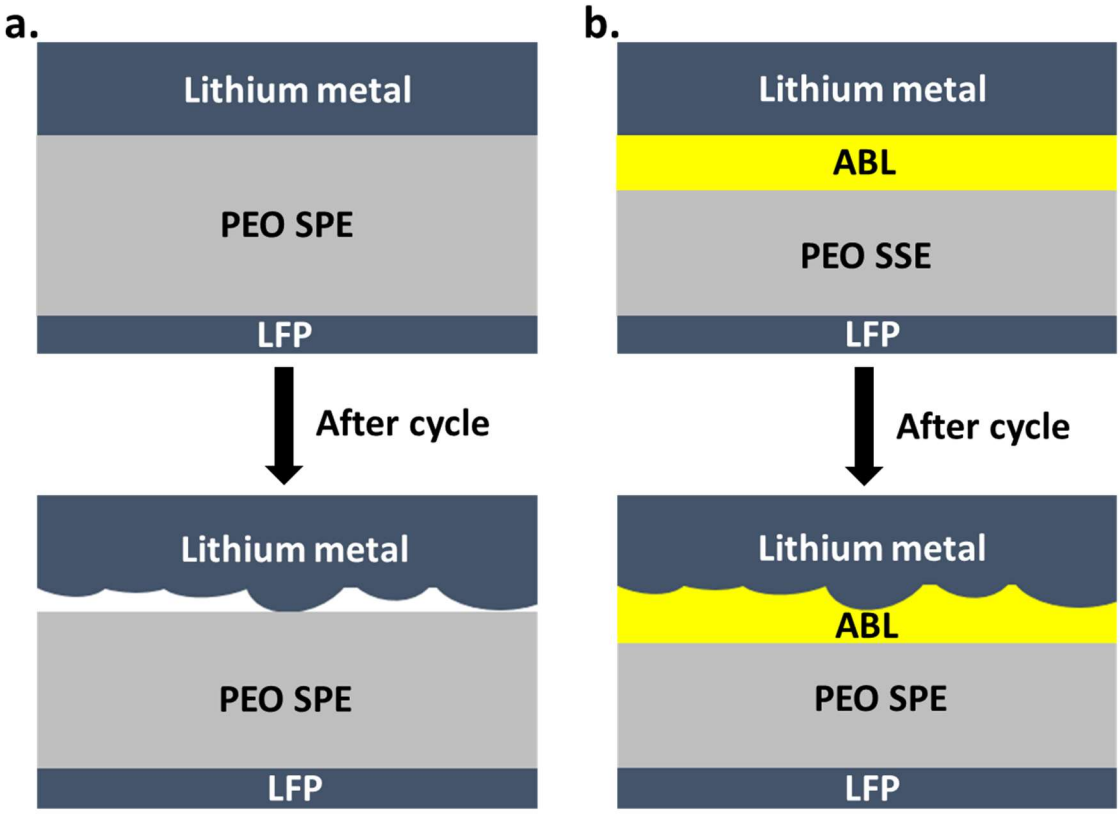

Figure 1.6. Schematic of the interface contact between Li metal anode and SPE before and after repeated cycles, (a) without and (b) with ABL.

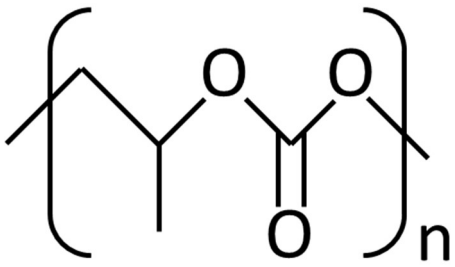

Figure 1.7. Structure of PPC.

CHAPTER 2. Experimental Section

2.1 Materials

Poly(ethylene oxide) (PEO, M.W. 600,000, Sigma-Aldrich), poly(propylene carbonate) (PPC, M.W. ~2000, Novomer Inc.), bis(trifluoromethane)sulfonimide lithium salt (LiTFSI, Sigma-Aldrich), acetonitrile (Alfa Aesar), $LiFePO_4$ powder (LFP, MTI Corporation), Super P (MTI Corporation).

2.2 Preparation of Solid Polymer Electrolyte Membrane (SPE) and Adaptive Buffer Layer (ABL)

PEO, PPC and LiTFSI were carefully dried at 60 °C overnight before use. PEO and LiTFSI were dissolved in acetonitrile (AN) and stirred for 24 h. The molar ratio of EO:Li was set to 8:1. After stirring, the SPE slurry containing PEO and LiTFSI was coated onto the stainless steel disk (0.001 in. thickness, TBI Corporation) or LFP cathode, and dried at 60 °C for 12 h to obtain samples for ionic conductivity or battery tests. The surface area of the stainless steel electrode for conductivity test is 0.785 cm^{-2}, and the thickness of SPE membrane is around 150 μm. To prepare the ABL, PEO, PPC and LiTFSI were dissolved in AN and stirred for 24 h. The mass ratio of PEO and PPC was set to 1:1, and the molar ratio of both of EO:Li and PC:Li were set to 8:1. After stirring for 24 h, the ABL solution was cast onto the stainless steel for conductivity tests or onto the top of SPE membrane for battery tests. The thickness of ABL is around 10 μm in the full battery. The above electrodes were transferred into an argon-filled glovebox and dried at 60 °C for 12 h.

2.3 Ionic Conductivity Measurments of SPEs

The ionic conductivities of the SPEs were measured by electrochemical impedance spectroscopy (EIS) with an AC amplitude of 10 mV in the frequency range of 1 MHz - 0.1 Hz. The measurments were performed on a Bio-Logic SAS at various temperatures ranging from 30 °C to 70 °C. The PEO and ABL were separately sandwiched between two stainless steel round disks inside a 2032 type coin cell for testing. The batteries were kept at each test temperature for 30 min to reach thermal equilibrium. The ionic conductivity (σ) of SPEs could be calculated by the resistance (R), the electrode area (S) and the electrode thickness (L), according to the following equation:

$$\sigma = L/(R \cdot S) \tag{4}$$

2.4 Electrochemical Test and Material Characterization

A composition of 60:20:12:8 of $LiFePO_4$/PEO/Super P/LiTFSI was used in the cathode slurry. These components were dispersed in AN and stirred overnight. The slurry was cast onto carbon-coated aluminum round disks with 1 cm diameter. After drying at 70 °C for 12 h, the LFP cathode was obtained. The mass loading of $LiFePO_4$ on the cathode ranged from 3.5 to 4.0 mg/cm^2. To get the cathode with SPE, the PEO SPE solution was directly cast onto the LFP cathode. After drying the SPE layer in a vacuum dryer overnight, they were transferred into the glovebox and heated at 70 °C for 12 h to remove the remaining trace of solvent. For the cathodes with ABL, the ABL solution was cast onto PEO SPE in the glovebox and dried for another 12 h. The full battery consisting of Li metal anode, SPE (with or without ABL) and LFP cathode were assembled into a 2031 coin cell inside the

glovebox. Batteries were cycled using an 8-channel (Wuhan LANHE electronics Corporation) battery tester in a temperature chamber (Tenney Environment, Thermal Product Solutions). To visualize the change of interfacial contact between Li metal and SPE, the battery was deeply discharged to 10 mAh at 0.04 mA/cm^2. The morphology of interfacial contact between Li metal and SPE after deep discharge was characterized by scanning electron microscopy (SEM, Hitachi 8230). All the tests of full batteries were conducted at 50 °C.

The total ionic conductivity measurements of full batteries were performed on a Bio-logic SAS. EIS measurements were performed at frequencies ranging from 1 MHz to 0.1 Hz before and after battery cycling at various temperatures (from 30 °C to 70 °C). The bulk resistance (R_b) and interface resistance (R_{int}) were fitted from the EIS curve. The total ionic conductivity (σ_t) of the full battery were calculated from the total resistance (R_t), the electrode area (S) and the electrode thickness (L), according to the following equation:

$$R_t = R_b + R_{int} \quad (5)$$

$$\sigma_t = L/(R_t \cdot S) \quad (6)$$

2.5 Rheological Measurements

A cone-plate geometry in an Anton Paar MCR 501 was used to measure the rheology. The diameter of the cone, the cone angle, and the truncation height is 25mm, 2 degrees, and 0.051mm, respectively. Frequency sweeps were performed at an applied strain amplitude of 0.1 at 50 °C.

CHAPTER 3. Results and Discussion

3.1 Fluidity of ABL

The ABL exhibits semi-liquid fluidity at 50 °C. PEO SPE, ABL and PPC SPE solutions were poured into three vials, dried for 24 hours in the fume hood at 70 °C, 12 h in the vacuum dryer and 12 h in the glovebox at 70 °C to completely remove the solvent. The vials were then laid horizontally on the bench. The PEO SPE showed nearly no fluidity and remained stuck to the bottom of the vial (Figure 3.1a). The ABL exhibited some fluidity and formed a sloped surface near the bottom of the vial (Figure 3.1b). However, the PPC SPE showed high fluidity and spread flat in the vial (Figure 3.1c). Besides, the surface condition of the cathode with ABL is obviously different from the one without ABL. In this work, LFP was used as cathode material of full batteries [34]. To reduce the interfacial resistance between SPEs and cathode, the SPE solution was directly cast onto the electrode. The surface conditions of the cathodes without and with ABL are obvious different. As shown in Figure 3.2a, the surface of the cathode without ABL was dark and uneven; on the contrary, the one with ABL was smooth and reflective (Figure 3.2b).

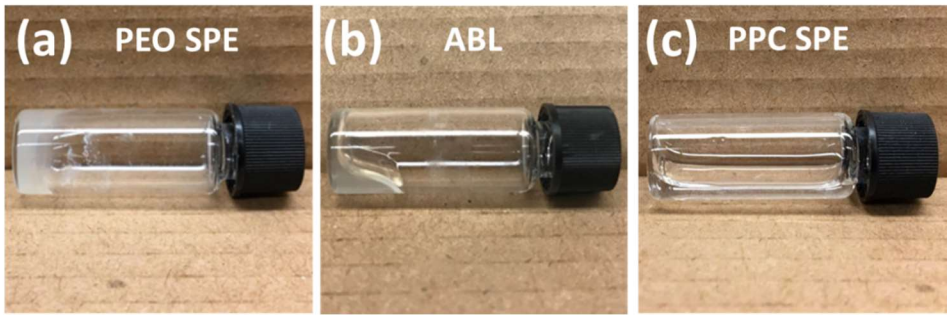

Figure 3.1. The completely dried (a) PEO SPE, (b) ABL, and (c) PPC SPE.

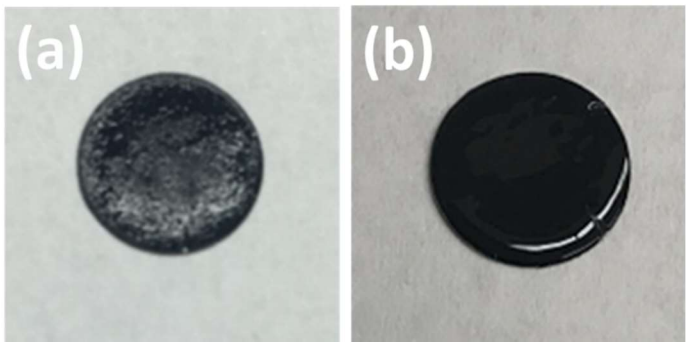

Figure 3.2. The surface conditions of the LFP cathodes with solid polymer electrolyte (a) without and (b) with ABL.

3.2 Viscoelastic Property of ABL

Viscoelasticity is the property of materials that exhibit both viscous and elastic characteristics while undergoing deformation. Viscous materials, like water, resist shear flow and strain linearly with time when a stress is applied. Elastic materials strain when stretched and immediately return to their original state once the stress is removed. Most materials are viscoelastic materials as they possess both viscous and elastic properties. A rheology test was used to measure the viscoelasticity of materials. A picture of the rheometer used is shown in Figure 3.3a, and a schematic of the rheometer is shown in Figure 3.3b. While testing the rheology, a specific strain rate is applied to the instrument. The stress response σ (t) of a viscoelastic material is given by,

$$\sigma(t) = G'(\omega)\Upsilon_0 \sin(\omega t) + G''(\omega)\Upsilon_0 \cos(\omega t) \quad (7)$$

Storage modulus, G'(ω), and loss modulus, G''(ω), characterize the solid-like and fluid-like contributions, respectively.

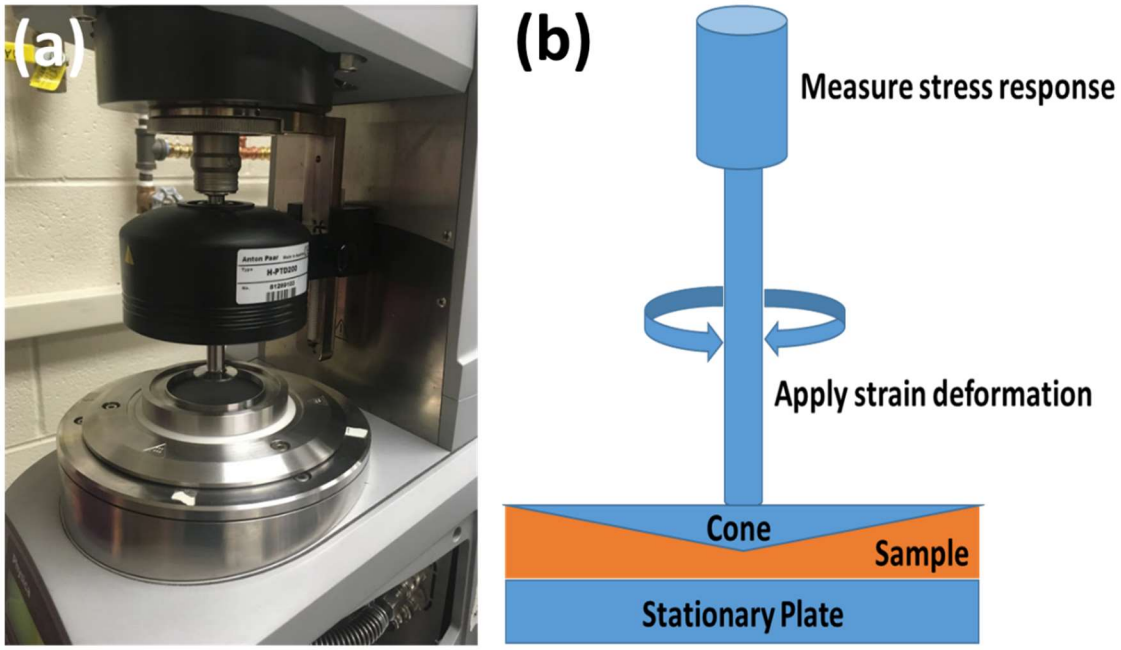

Figure 3.3. (a) Picture of the rheometer. (b) Schematic of the rheometer.

To quantify the viscoelastic properties of PEO SPE and ABL, rheology experiments were carried out by rheometer with various strain rates at 50 °C. For a given viscoelastic sample, when the strain rate is low, viscous characteristics will dominate, and the materials will behave more like a liquid; when strain rate is high, elastic property will dominate. Figure 3.4a and 3.4b show the results of rheological measurement of PEO SPE and ABL, respectively. The intersection value of storage modulus and loss modulus of PEO SPE is ~ 0.033 s^{-1}, and that of ABL is ~ 0.12 s^{-1}. Since the intersection value of ABL was higher than that of PEO SPE, the ABL behaves like a liquid more [35].

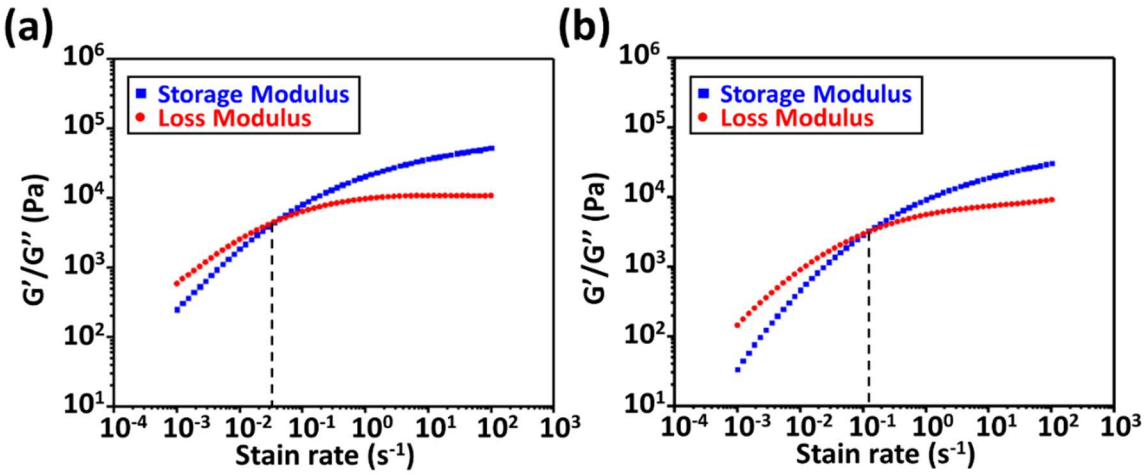

Figure 3.4. Characterization of the viscoelastic property with rheological study of (a) PEO SPE, and (b) ABL.

3.3 Ionic Conductivities

For SPEs, high ionic conductivity and capacity retention over battery cycling are of vital importance. At the same current density, the battery with higher ionic conductivity will have lower ohmic voltage loss, more complete reactions, and higher specific capacity of electrode material. The ion conductivity was measured by EIS in a 2032 type coin cell, in which the SPE and ABL/SPE were sandwiched between two stainless steel disks. Figure 3.5 shows the schematic of the coin cell structure of the ionic conductivity test.

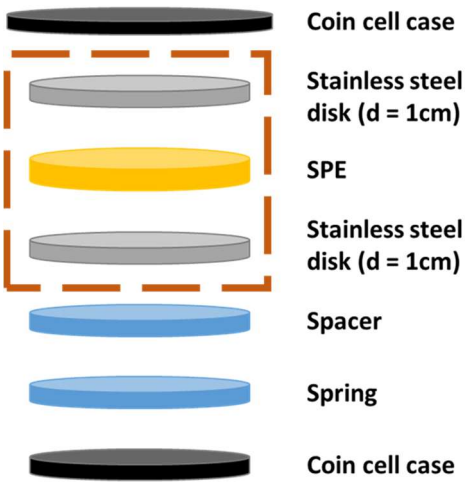

Figure 3.5. Schematic of the structure of the battery for ionic conductivity test.

The ionic conductivity tests of PEO SPE and ABL were carried out at various temperatures, ranging from 30 °C to 70 °C. Due to the virtue of the low T_g, PPC is supposed to increase the ionic conductivity of ABL [14]. As shown in Figure 3.6, the results are consistent with our hypothesis. The ABL has higher ionic conductivity than PEO SPE at all measured temperatures.

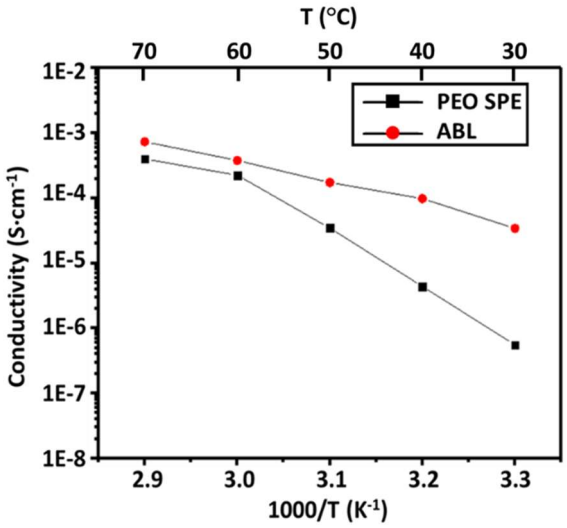

Figure 3.6. Arrhenius plots of the conductivity of PEO SPE and ABL.

In an as-made battery containing solid electrolyte, the overall voltage ohmic loss is related to the mobility of Li^+ and the number of carriers in the solid electrolyte. After battery cycling, however, the surface deformation of lithium metal anode will cause the loss of intimate contact between the anode and the solid electrolyte. The poor interfacial contact deteriorates lithium ion transport and decreases the overall ionic conductivity. On the other hand, ABL is able to maintain good interfacial contact between Li metal anode and SPE, keeping the interface resistance of the full battery from increasing during battery cycling. To study the change of interfacial contact before and after battery cycling, we assembled and tested (at 50 °C and 1C rate) Li/SPE/$LiFePO_4$ and Li/ABL/SPE/$LiFePO_4$ full batteries. The structure of the batteries is shown in Figure 3.7.

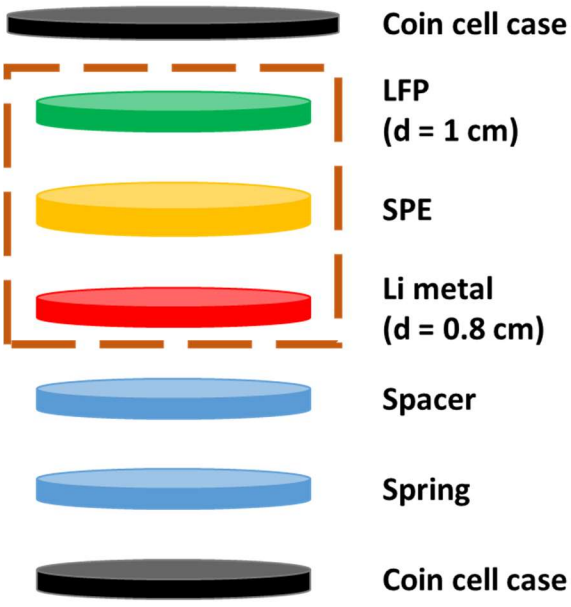

Figure 3.7. Schematic of the structure of the battery.

The interface resistance of the full battery was measured by EIS before and after 150 cycles. Figure 3.8 shows the fitting results of EIS at 50 °C and inset of the figure demonstrates the equivalent circuit model for the impedance spectra [36]. R_e and R_{int} represent the bulk resistance and interface resistance, respectively. The interfac resistance increased drastically, from 202 Ω to 439 Ω (117%), for the battery without ABL; in contrast, there was only a 20% increase, from 156 Ω to 187 Ω, for the one with ABL. Furthermore, the EIS tests were carried out at various temperatures, from 30 °C to 70 °C, to measure the total conductivity of full battery which are calculated from total resistance (R_t) according to equation (6). The R_t is the sum of bulk resistance (R_b) and interfac resistance (R_{int}). The total conductivity of the full battery was shown in Figure 3.9a and 3.9b. The battery without ABL had an obvious decay of conductivity after cycling as indicated by the blue arrow in Figure 3.9a. In contrast, there was nearly no change in the ionic conductivity of the battery with ABL, indicating the ABL has great impact on ionic conductivity retention.

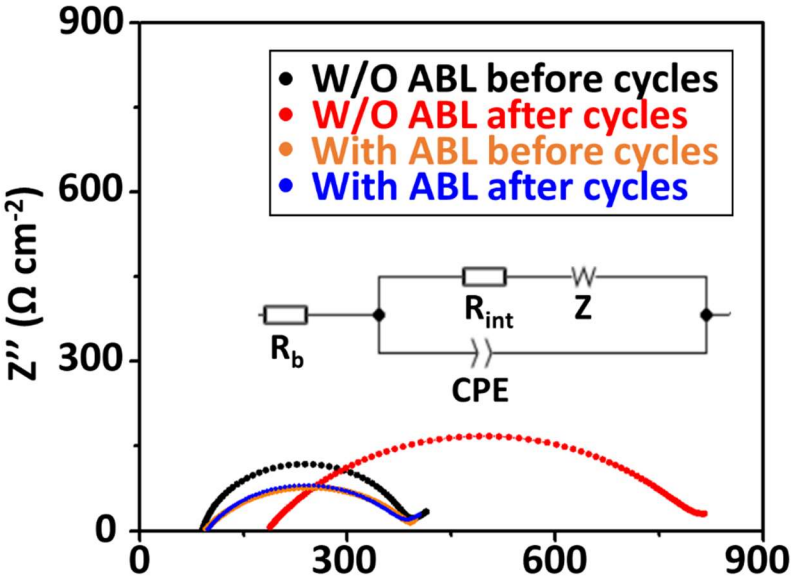

Figure 3.8. Nyquist plots of full batteries at 50 °C.

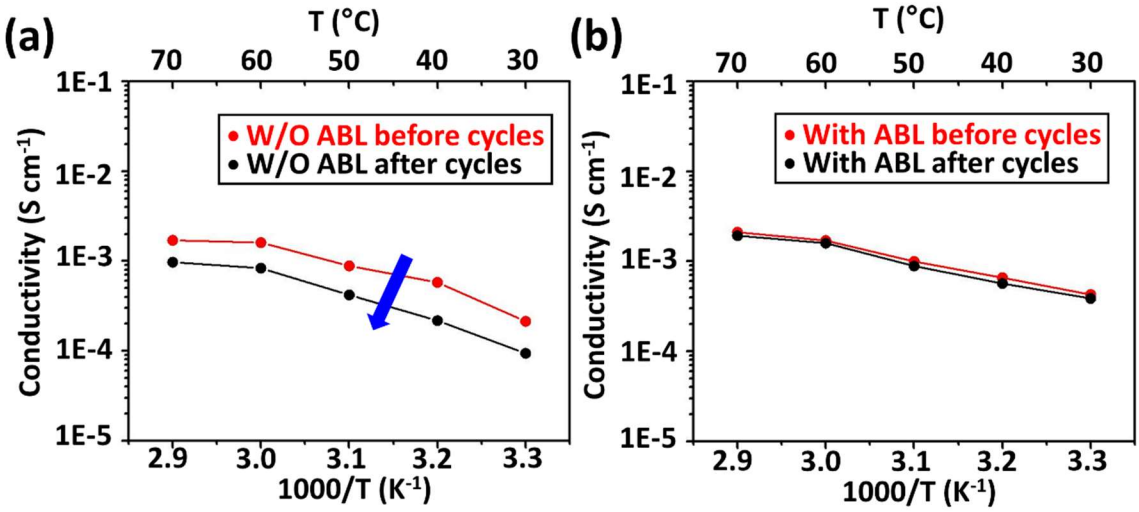

Figure 3.9. Arrhenius plots of the conductivities of full batteries (a) Li/SPE/$LiFePO_4$, (b) Li/ABL/SPE/$LiFePO_4$ before and after 150 cycles.

3.4 Electrochemical Performance

The rate capabilities of the Li/SPE/$LiFePO_4$ batteries were presented in Figure 3.10. The battery with ABL shows good capacity retention, and obviously higher specific capacities at various current rates than the one without ABL.

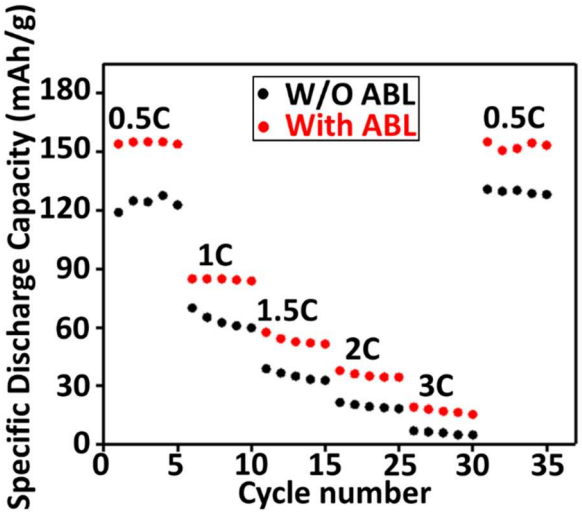

Figure 3.10. Comparison of the rate performance of Li/SPE/LFP batteries with and without ABL.

Figure 3.11a and 3.11b show the charge-discharge voltage profiles. With the increase of the current density, the voltage platform gradually becomes shorter, because of the polarization effect of cathode at high current densities [37]. The battery with ABL was able to deliver higher capacity than the one without ABL.

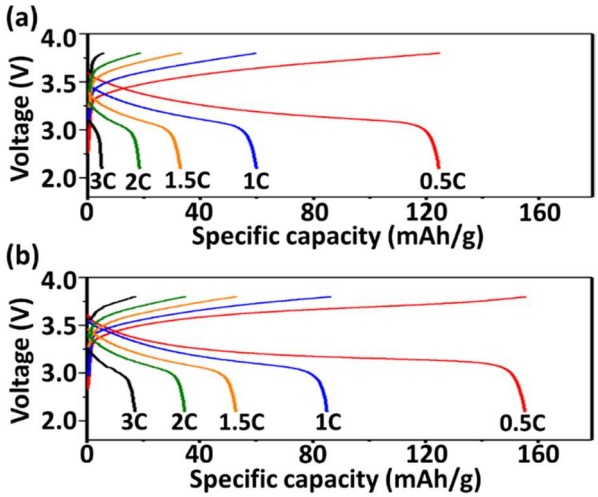

Figure 3.11. Charge and discharge voltage vs. discharge specific capacity profiles of Li/SPE/LFP at various rates (a) without, and (b) with ABL.

Capacity retention and Coulombic efficiency of batteries at 1 C and 50 °C were shown in Figure 3.12a and 3.12b. The initial discharge specific capacities of the batteries with and without ABL were 110 mAh/g and 60 mAh/g, respectively.

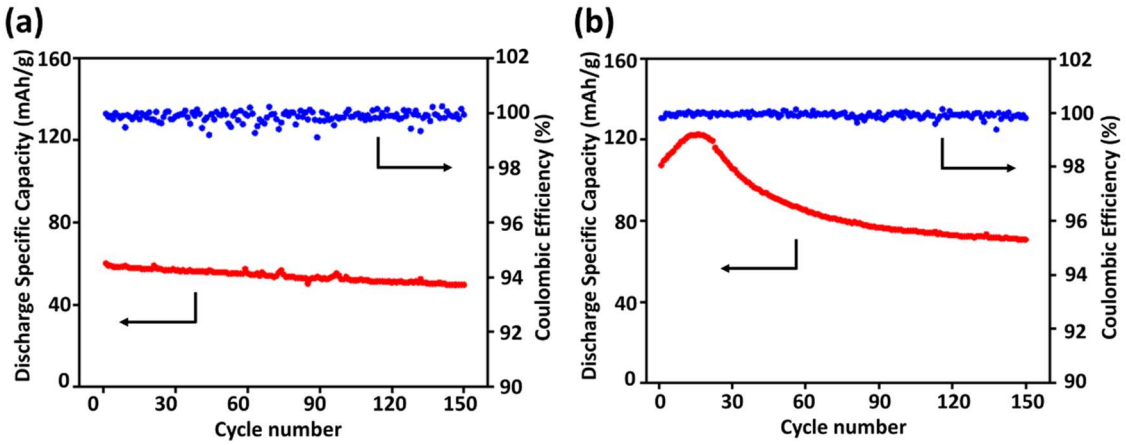

Figure 3.12. The capacity retentions and Coulombic efficiency at 1 C, 50 °C, (a) without and (b) with ABL.

To visualize change of the interfacial contact between Li metal anode and SPE, a deep discharge of the Li/SPE/Li symmetric cell to 20 mAh/cm^2 was run at a low current density, 0.04 mA/cm^2. Figure 3.13a shows the SEM image of the cross section of the battery without ABL after deep discharge where the obvious gaps between lithium metal anode and SPE were observed; in contrast, the battery with ABL still kept good interfacial contact (Figure 3.13b).

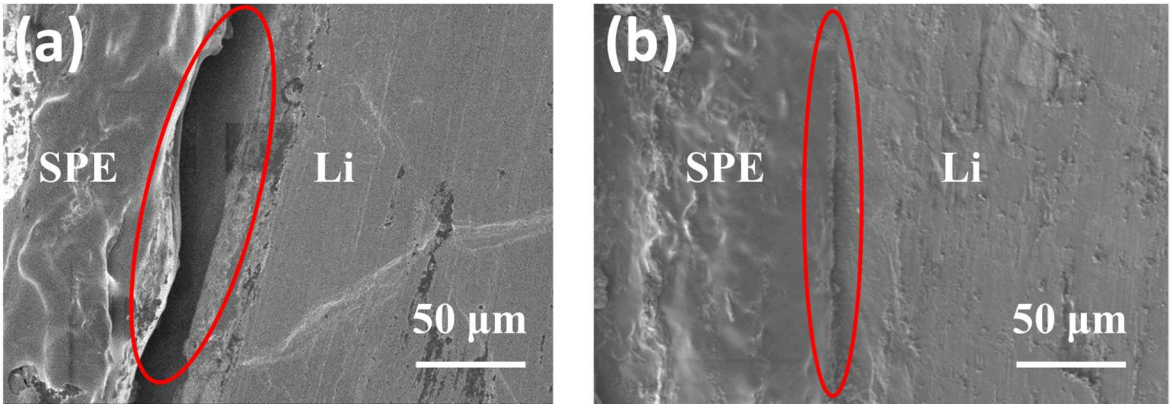

Figure 3.13. SEM images of the cross section for Li/SPE/LFP batteries after deep discharge to 10 mAh/cm^2 at 0.04 mA/cm^2 current density (a) without and (b) with ABL.

CHAPTER 4. Conclusion and Perspective

In summary, we have successfully designed and fabricated an ABL to improve the interfacial contact between the Li metal anode and SPE, and to maintain good interfacial contact during battery cycling. From the rheology test, ABL showed better liquid-like properties at 50 °C, which helped the SPE adapt to the shape change of the anode during battery cycling. After cycling, the increase in interface resistance for the battery with ABL (20%) was lower than the one without ABL (117%). Due to the improved interfacial contact between Li and SPE, the initial specific discharge capacity of Li/ABL/SPE/LFP battery (110 mAh/g) was nearly twice that of the battery without ABL (60 mAh/g). Besides, since ABL is able to keep good interfacial contact, the battery with ABL delivers more stable Coulumbic efficiency during battery cycling. Our work offers a new way to maintain stable interfaces between dimensionally changing electrodes and electrolyte, particularly for all-solid-state batteries.

REFERENCES

(1) Dunn, B.; Kamath, H.; Tarascon, J.-M. J. S. Electrical energy storage for the grid: a battery of choices. *Science* **2011**, *334*, 928-935.

(2) Yang, Z.; Zhang, J.; Kintner-Meyer, M. C.; Lu, X.; Choi, D.; Lemmon, J. P.; Liu, J. J. C. r. Electrochemical energy storage for green grid. *Chem. Rev.* **2011**, *111,* 3577-3613.

(3) Padhi, A. K.; Nanjundaswamy, K. S.; Goodenough, J. B. J. J. o. t. e. s. Phospho-olivines as positive-electrode materials for rechargeable lithium batteries. *J. Electrochem. Soc.* **1997**, *144,* 1188-1194.

(4) Lin, D.; Liu, Y.; Cui, Y. Reviving the lithium metal anode for high-energy batteries. *Nat. Nanotechnol.* **2017**, *12,* 194-206.

(5) Cheng, X. B.; Zhang, R.; Zhao, C. Z.; Zhang, Q. Toward Safe Lithium Metal Anode in Rechargeable Batteries: A Review. *Chem. Rev.* **2017**, *117,* 10403-10473.

(6) Manthiram, A.; Yu, X.; Wang, S. Lithium battery chemistries enabled by solid-state electrolytes. *Nat. Rev. Mater.* **2017**, *2,* 16103.

(7) Liu, W.; Liu, N.; Sun, J.; Hsu, P. C.; Li, Y.; Lee, H. W.; Cui, Y. Ionic conductivity enhancement of polymer electrolytes with ceramic nanowire fillers. *Nano Lett.* **2015**, *15,* 2740-5.

(8) Busche, M. R.; Drossel, T.; Leichtweiss, T.; Weber, D. A.; Falk, M.; Schneider, M.; Reich, M. L.; Sommer, H.; Adelhelm, P.; Janek, J. Dynamic formation of a solid-liquid

electrolyte interphase and its consequences for hybrid-battery concepts. *Nat. Chem.* **2016**, *8,* 426-434.

(9) El-Shinawi, H.; Regoutz, A.; Payne, D. J.; Cussen, E. J.; Corr, S. A. NASICON LiM2(PO4)3 electrolyte (M = Zr) and electrode (M = Ti) materials for all solid-state Li-ion batteries with high total conductivity and low interfacial resistance. *J. Mater. Chem. A* **2018**, *6,* 5296-5303.

(10) Han, X.; Gong, Y.; Fu, K. K.; He, X.; Hitz, G. T.; Dai, J.; Pearse, A.; Liu, B.; Wang, H.; Rubloff, G.; Mo, Y.; Thangadurai, V.; Wachsman, E. D.; Hu, L. Negating interfacial impedance in garnet-based solid-state Li metal batteries. *Nat. Mater.* **2017**, *16,* 572-579.

(11) Kamaya, N.; Homma, K.; Yamakawa, Y.; Hirayama, M.; Kanno, R.; Yonemura, M.; Kamiyama, T.; Kato, Y.; Hama, S.; Kawamoto, K.; Mitsui, A. A lithium superionic conductor. *Nat. Mater.* **2011**, *10,* 682-686.

(12) Kato, Y.; Hori, S.; Saito, T.; Suzuki, K.; Hirayama, M.; Mitsui, A.; Yonemura, M.; Iba, H.; Kanno, R. High-power all-solid-state batteries using sulfide superionic conductors. *Nat. Energy* **2016**, *1,* 16030.

(13) Wright, P. V. Electrical Conductivity in Ionic Complexes of Poly(ethylene oxide). *Br. Polym. J.* **1975**, 7, 319-327.

(14) Zhang, J.; Yang, J.; Dong, T.; Zhang, M.; Chai, J.; Dong, S.; Wu, T.; Zhou, X.; Cui, G. Aliphatic Polycarbonate-Based Solid-State Polymer Electrolytes for Advanced Lithium Batteries: Advances and Perspective. *Small* **2018**, *14*, 1800821.

(15) Li, J.; Lin, Y.; Yao, H.; Yuan, C.; Liu, J. Tuning thin-film electrolyte for lithium battery

by grafting cyclic carbonate and combed poly(ethylene oxide) on polysiloxane. *ChemSusChem.* **2014**, *7,* 1901-1908.

(16) Nagaoka, K.; Naruse, H.; Shinohara, I.; Watanabe, M. High ionic conductivity in poly (dimethyl siloxane-co-ethylene oxide) dissolving lithium perchlorate. *J. Polym. Sci., Polym. Lett. Ed.* **1984**, *22,* 659-663.

(17) Fish, D.; Khan, I. M.; Smid, J. J. D. M. C., Rapid Communications. Conductivity of solid complexes of lithium perchlorate with poly{[ω-methoxyhexa (oxyethylene) ethoxy] methylsiloxane}. *Macromol. Rapid Commun.* **1986**, *7,* 115-120.

(18) Ma, Q.; Zhang, H.; Zhou, C.; Zheng, L.; Cheng, P.; Nie, J.; Feng, W.; Hu, Y. S.; Li, H.; Huang, X.; Chen, L.; Armand, M.; Zhou, Z. Single Lithium-Ion Conducting Polymer Electrolytes Based on a Super-Delocalized Polyanion. *Angew. Chem., Int. Ed.* **2016**, *55,* 2521-2525.

(19) Bannister, D. J.; Davies, G. R.; Ward, I. M.; McIntyre, J. E. Ionic conductivities for poly (ethylene oxide) complexes with lithium salts of monobasic and dibasic acids and blends of poly (ethylene oxide) with lithium salts of anionic polymers. *Polymer* **1984**, *25,* 1291-1296.

(20) Bouchet, R.; Maria, S.; Meziane, R.; Aboulaich, A.; Lienafa, L.; Bonnet, J.-P.; Phan, T. N.; Bertin, D.; Gigmes, D.; Devaux, D. J. N. m. Single-ion BAB triblock copolymers as highly efficient electrolytes for lithium-metal batteries. *Nat. Mater.* **2013**, *12,* 452-457.

(21) Xue, Z.; He, D.; Xie, X. Poly(ethylene oxide)-based electrolytes for lithium-ion batteries. *J. Mater. Chem. A* **2015**, *3,* 19218-19253.

(22) Croce, F.; Persi, L.; Scrosati, B.; Serraino-Fiory, F.; Plichta, E.; Hendrickson, M. J. E. A. Role of the ceramic fillers in enhancing the transport properties of composite polymer electrolytes. *Electrochim. Acta* **2001**, *46,* 2457-2461.

(23) Lin, D.; Liu, W.; Liu, Y.; Lee, H. R.; Hsu, P.-C.; Liu, K.; Cui, Y. J. N. l. High ionic conductivity of composite solid polymer electrolyte via in situ synthesis of monodispersed SiO2 nanospheres in poly (ethylene oxide). 2015, 16 (1), 459-465.

(24) Xiong, H.-M.; Wang, Z.-D.; Xie, D.-P.; Cheng, L.; Xia, Y.-Y. Stable polymer electrolytes based on polyether-grafted ZnO nanoparticles for all-solid-state lithium batteries. *J. Mater. Chem.* **2006**, *16,* 1345-1349.

(25) Zhao, C. Z.; Zhang, X. Q.; Cheng, X. B.; Zhang, R.; Xu, R.; Chen, P. Y.; Peng, H. J.; Huang, J. Q.; Zhang, Q. An anion-immobilized composite electrolyte for dendrite-free lithium metal anodes. *Proc. Natl. Acad. Sci. U.S.A.* **2017**, *114,* 11069-11074.

(26) Wang, W.; Yi, E.; Fici, A. J.; Laine, R. M.; Kieffer, J. Lithium Ion Conducting Poly(ethylene oxide)-Based Solid Electrolytes Containing Active or Passive Ceramic Nanoparticles. The *J. Phys. Chem. C* **2017**, *121,* 2563-2573.

(27) Wan, J.; Xie, J.; Mackanic, D. G.; Burke, W.; Bao, Z.; Cui, Y. Status, promises, and challenges of nanocomposite solid-state electrolytes for safe and high performance lithium batteries. *Materials Today Nano* **2018**, *4,* 1-16.

(28) Feuillade, G.; Perche, P. Ion-conductive macromolecular gels and membranes for solid lithium cells. *J. Appl. Electrochem.* **1975**, *5,* 63-69.

(29) Zhao, Y.; Zhang, Y.; Sun, H.; Dong, X.; Cao, J.; Wang, L.; Xu, Y.; Ren, J.; Hwang,

Y.; Son, I. H.; Huang, X.; Wang, Y.; Peng, H. A Self-Healing Aqueous Lithium-Ion Battery. *Angew. Chem. Int. Ed.* **2016**, *55*, 14384-14388.

(30) Wang, C.; Wu, H.; Chen, Z.; McDowell, M. T.; Cui, Y.; Bao, Z. Self-healing chemistry enables the stable operation of silicon microparticle anodes for high-energy lithium-ion batteries. *Nat. Chem.* **2013**, *5*, 1042-1408.

(31) Lin, D.; Yuen, P. Y.; Liu, Y.; Liu, W.; Liu, N.; Dauskardt, R. H.; Cui, Y. A Silica-Aerogel-Reinforced Composite Polymer Electrolyte with High Ionic Conductivity and High Modulus. *Adv. Mater.* **2018**, *30,* 1802661.

(32) Zhang, J.; Zhao, J.; Yue, L.; Wang, Q.; Chai, J.; Liu, Z.; Zhou, X.; Li, H.; Guo, Y.; Cui, G.; Chen, L. Safety-Reinforced Poly(Propylene Carbonate)-Based All-Solid-State Polymer Electrolyte for Ambient-Temperature Solid Polymer Lithium Batteries. *Adv. Energy Mater.* **2015**, *5,* 1501082.

(33) Deng, K.; Wang, S.; Ren, S.; Han, D.; Xiao, M.; Meng, Y. A Novel Single-Ion-Conducting Polymer Electrolyte Derived from CO2-Based Multifunctional Polycarbonate. *ACS Appl. Mater. Interfaces* **2016**, *8,* 33642-33648.

(34) Li, Y.; Xu, B.; Xu, H.; Duan, H.; Lu, X.; Xin, S.; Zhou, W.; Xue, L.; Fu, G.; Manthiram, A.; Goodenough, J. B. Hybrid Polymer/Garnet Electrolyte with a Small Interfacial Resistance for Lithium-Ion Batteries. *Angew. Chem. Int. Ed.* **2017**, *56,* 753-756.

(35) Liu, K.; Pei, A.; Lee, H. R.; Kong, B.; Liu, N.; Lin, D.; Liu, Y.; Liu, C.; Hsu, P. C.; Bao, Z.; Cui, Y. Lithium Metal Anodes with an Adaptive "Solid-Liquid" Interfacial Protective Layer. *J. Am. Chem. Soc.* **2017**, *139,* 4815-4820.

(36) Lu, Q.; He, Y. B.; Yu, Q.; Li, B.; Kaneti, Y. V.; Yao, Y.; Kang, F.; Yang, Q. H. Dendrite-Free, High-Rate, Long-Life Lithium Metal Batteries with a 3D Cross-Linked Network Polymer Electrolyte. *Adv. Mater.* **2017**, *29,* 1604460.

(37) Zeng, H.; Ji, X.; Tsai, F.; Zhang, Q.; Jiang, T.; Li, R. K. Y.; Shi, H.; Luan, S.; Shi, D. Enhanced cycling performance for all-solid-state lithium ion battery with LiFePO4 composite cathode encapsulated by poly (ethylene glycol) (PEG) based polymer electrolyte. *Solid State Ionics* **2018**, *320,* 92-99.